Grain size, orientation and source density study of dislocation configurational energy density

Zebang Zheng *[a], Fionn P.E. Dunne [b]

a. State Key Laboratory of Solidification Processing, Shaanxi Key Laboratory of High-Performance Precision Forming Technology and Equipment, School of Materials Science and Engineering, Northwestern Polytechnical University, Xi'an 710072, China

b. Department of Materials, Imperial College London, London SW7 2AZ, United Kingdom

Abstract

The effects of grain size, source density and misorientations on the dislocation configurational energy area density are investigated using two-dimensional discrete dislocation plasticity. Grain boundaries are modelled as impenetrable to dislocations. The considered grain size varies from $0.4\mu m^2$ to $8.0\mu m^2$. The configurational energy area density displays a strong size dependence similar to the stress response. Two sets of materials are considered: low and high source/obstacle density. The high source density specimens result in a negative configurational energy which implies the dislocation structure is more stable than for isolated dislocations. The contribution from misorientation to the configurational energy density is analysed using specimens with single orientation and a checker-board arrangement. The configurational energy density is found not only to depend on the dislocation spacing but is also related to the local stress states. Low source densities lead to higher (positive) configurational energy densities.

Keywords: Configurational Energy; Discrete Dislocation Plasticity; Size Effect; Misorientations; Source Density

* *Corresponding author: zebang.zheng@nwpu.edu.cn* (Z.Zheng)

1. Introduction

During plastic deformation of metals, some of the work done is transferred to free energy stored in the material of which a considerable fraction is stored in the dislocation structure which evolves with loading. Independent studies have shown that the resulting dislocation structure energy density may be important in fatigue crack nucleation and the microstructurally-sensitive growth of the cracks. These may be captured with the higher length scale crystal plasticity quantity termed stored energy density which has been shown to be related to the dislocation configurational energy density, potentially providing the multiscale link from dislocation structure to crystal plasticity fatigue. Hence the sensitivity of the configurational energy density to key microstructural features including dislocation source density, grain size and misorientation is of interest for higher length scale fatigue behaviour.

Modelling techniques at the dislocation length scale, which include discrete dislocation plasticity (DDP) as an example, provide a powerful tool to analyse the local energy associated with dislocation activities. Plastic flow in DDP arises from the collective motion of dislocations which are governed by a set of constitutive rules. The inclusion of individual dislocation behaviour enables the calculation of spatial energy distributions. Ghoniem and co-authors [1,2] presented the energy development during dislocation motion using 3D DDP modelling. Zbib et al. [3,4] discussed the elastic stored energy within dislocation arrays due to the dislocation interactions in 3D DDP simulations. Deshpande et al. [5,6] introduced the method in 2D DDP to calculate the energy stored in dislocation structure. Benzerga et al. [7] systematically analysed the fraction of elastic stored energy, dissipated energy and the energy in dislocation structure for uniaxial tension. Their results suggest that the ratio of stored energy in their material to the plastic work is between 0.05 to 0.2. Zheng et al. [8] recently introduced the configurational energy density which is associated with the dislocation interactions. This term is different to the energy stored in the dislocation structure which also contains the dislocation self energy and core energy. The configurational energy density in DDP provides underpinning insight into the higher level crystal plasticity quantity called stored energy density [9] which has been demonstrated to capture accurately the site of fatigue crack nucleation [10], the cycles to crack nucleation [11], and the microstructure-sensitive growth paths [12] and rates of growth in BCC, FCC and HCP metals [13]. There are several modelling parameters in DDP which are potentially important in determining the plastic behaviour and hence the energy distribution. The aim of the present study is thus to investigate the role of the uncertainties of three modelling parameters, i.e. grain size, source density and misorientation, in the calculation of configurational energy density.

Size-dependent response has been widely investigated using DDP because the length scale is naturally incorporated in the displacement and stress field of dislocation. Extensive work has been carried out using 3D DDP models in both single crystal and polycrystals. Devincre et al. [14] used 3D DDP simulations to establish a dislocation-based continuum model and their multiscale methodology can be used to study size effects in small dimensions. Rao et al. [15] established numerous 3D DDP simulations to investigate the athermal size-dependent strengthening in microcompression. El-Awady et al. [16] developed a self-consistent boundary element-dislocation dynamics framework to examine the influence of free surfaces on dislocation motion in an FCC single crystal. El-Awady [17] later utilised 3D DDP simulations to study the Hall–Petch relationship in polycrystals. For the two-dimensional approaches, Deshpande et al. [5] analysed the compressive and tensile responses of a single crystal with single slip system under plane strain conditions and Balint et al. [14] compares the size-dependent tensile responses of single and polycrystals. Kondori et al. [15] studied the size effects in tapered micropillars, Tarleton et al. [16] studied micro-cantilever bending DDP results against experiments and Balint et al. [17] investigated the size dependence of nanoindentation. Cleveringa et al. [18] investigated the bending response of different sized specimens, and Quek et al. [19] observed the inverse Hall-Petch

relation in nanocrystalline metals using DDP. The aforementioned studies indicate that the size effect is an important aspect in affecting the stress responses under various loading conditions. Hence it is important to study how it affects the configurational energy density which in turn underpins the crystal plasticity stored energy density demonstrated to be important in the nucleation and microstructurally-senstive growth of fatigue cracks [10,12,13,20].

On the other hand, the source/obstacle density and crystal orientation also significantly influence the plasticity, especially the hardening behaviour. Balint et al. [14] compares the dislocation density evolution and stress responses of single and polycrystals with different source and obstacle densities. Biner and Morris [21] studied the effects of source density on the strengthening behaviour of polycrystals and found that the source density and location do not affect the Hall-Petch relationship within their considered grain size range. A high source density is assumed in the micropillar compression DDP simulations [15] to ensure similar yield strengths in different sample sizes. Except the overall responses, the local stress in one grain is experimentally observed to be significantly affected by its immediate neighbour [22,23]. Since the configurational energy density depends on both global and local stress states, the effects from source density and misorientations in neighbouring grains are also potentially important and are addressed here.

Two-dimensional calculations are carried out for planar polycrystalline specimens subject to uniaxial deformation. The DDP formulation and the methodology of calculating configurational energy area density are described in Section 2. The effects of grain size, source density and misorientations are investigated and discussed in Section 3. Finally in Section 4, concluding remarks are presented.

2. Discrete dislocation plasticity formulation

2.1 DDP framework and model

A two-dimensional plane strain model with regular hexagonal grains as shown in Fig. 1 is built for DDP simulations of uniaxial tension behaviour of polycrystals of thickness 4μm and length 12μm. Plasticity arises from the collective motion of discrete edge dislocations on specified slip planes. The boundary conditions are shown schematically in Fig. 1 where the left surface of the model is constrained along the x-direction and a displacement-controlled stretch with a constant strain of $\dot{\varepsilon} = 2000s^{-1}$ is applied on the right. The top and bottom surfaces of the model are traction free and dislocations are able to escape from these surfaces.

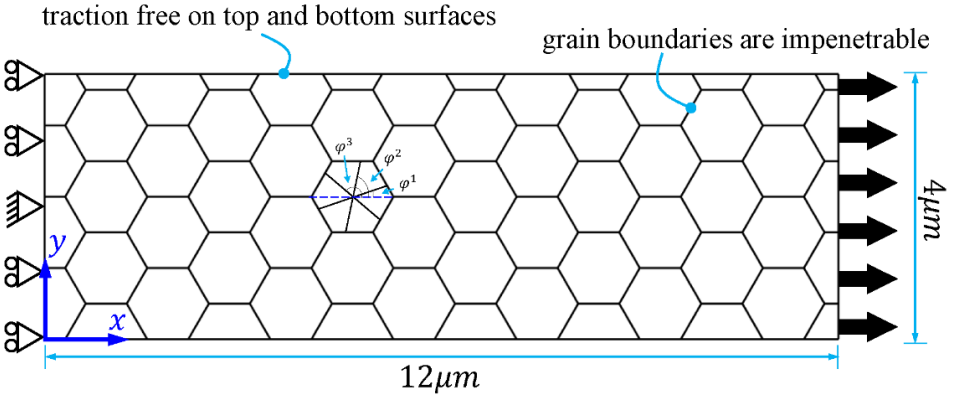

Fig. 1. Schematic diagram of the boundary value problem of the analysed uniaxial tension.

The classic superposition method [24] for solving small strain boundary value problem is adopted in the present study. The material properties are chosen from the literature [5,14,17,25,26] to be representative of metals like aluminium which have been widely used for DDP simulations, but the methodology can be generalised to other material systems. The considered polycrystal is elastically isotropic with Young's modulus $E = 70\text{GPa}$ and Poisson's ratio $\nu = 0.33$. Three potentially active slip systems at angles $\varphi^{(i)}(i = 1, 2, 3)$ with respect to the positive x-axis, where the angle between the neighbouring system is 54.75^{o}, are predefined to model the crystal orientations for plane strain loading in BCC crystals [27]. The specimen is dislocation-free prior to loading and Frank-Read sources and obstacles are randomly distributed on the predefined slip systems of each grain. The source strength τ_{nuc} is assigned from a Gaussian distribution with an average value of $\bar{\tau}_{nuc} = 50\text{MPa}$ and a standard deviation of 1MPa. In order to eliminate the effect from the random spatial distribution of sources/obstacles and the Gaussian distribution of source strength, for each set of parameters considered in the current study, three simulations were carried out but only one of them was chosen to present. Note that although the fluctuations of the overall stress-strain responses and the resultant dislocation structures are slightly different in the three simulations, the findings presented in the paper are not affected by the randomness of the sources/obstacles. The strength of obstacles is $\tau_{obs} = 150\text{MPa}$ beyond which dislocations are able to pass through. We consider two sets of source/obstacle densities as in [14] for parameter study: a low source density (LSD) of $\rho_{nuc} = \rho_{obs} = 56\mu m^{-2}$ and a high source density (HSD) of $\rho_{nuc} = 200\mu m^{-2}$ and $\rho_{obs} = 100\mu m^{-2}$. The average source and obstacle spacing thus can be determined as $d_{nuc} = 1/\sqrt{\rho_{nuc}}$ and $d_{obs} = 1/\sqrt{\rho_{obs}}$ respectively, i.e. $d_{nuc} = d_{obs} = 0.13\mu m$ for LSD and $d_{nuc} = 0.07\mu m$, $d_{obs} = 0.10\mu m$ for HSD. The strength of obstacles and sources for LSD and HSD obeys the same rule as described earlier, i.e. $\tau_{obs} = 3\bar{\tau}_{nuc} = 150\text{MPa}$. The effect of source/obstacle strength in the DDP model is also investigated by Benzerga et al. [28] and Chakravarthy and Curtin [29]. Edge dislocations with Burgers vector $\boldsymbol{b}$ ($|b|$=0.25nm) are emitted from the sources when the local resolved shear stress exceeds the source strength over a period of emission time $t_{nuc} = 10\text{ns}$.

The displacement $\boldsymbol{u}$, strain $\boldsymbol{\varepsilon}$ and stress $\boldsymbol{\sigma}$ are computed at each increment during loading according to [24] as

$$\boldsymbol{u} = \tilde{\boldsymbol{u}} + \hat{\boldsymbol{u}}\,, \quad \boldsymbol{\varepsilon} = \tilde{\boldsymbol{\varepsilon}} + \hat{\boldsymbol{\varepsilon}}\,, \quad \boldsymbol{\sigma} = \tilde{\boldsymbol{\sigma}} + \hat{\boldsymbol{\sigma}} \tag{1}$$

in which the ~ field donates the sum of individual dislocation fields within an infinite matrix medium and the $\hat{}$ field donates the smooth image field for the correction of actual boundary conditions. The gliding of dislocations along their slip planes are governed by the mobility law given as

$$\boldsymbol{v}^{(i)} = \frac{\boldsymbol{f}^{(i)}}{B} \tag{2}$$

where $B = 10^{-4}\text{Pa}\cdot\text{s}$ is the drag coefficient and $\boldsymbol{f}^{(i)}$ the Peach-Koehler force acting on the dislocation i written as

$$\boldsymbol{f}^{(i)} = \boldsymbol{n}^{(i)} \cdot \left(\hat{\boldsymbol{\sigma}} + \sum_{j \neq i} \tilde{\boldsymbol{\sigma}}^{(j)} \right) \cdot \boldsymbol{b}^{(i)} \tag{3}$$

where $\boldsymbol{n}^{(i)}$ is the unit vector of the normal to the slip plane. Two opposite-signed dislocations on the same slip plane annihilate with each other when they are within a critical distance $L_e = 6b$. In order to resolve the dislocation structure, a time step $\Delta t = 0.5\text{ns}$ is used.

The grain size considered in the present study varies from $0.4\mu\text{m}^2$ to $8.0\mu\text{m}^2$. The effect of penetrability of grain boundaries in HCP titanium alloys [30] and FCC aluminium alloys [31] with respect to misorientations between neighbouring grains has been quantitatively investigated in previous studies. The results suggest that the flow stress under high strain rates is lower when slip transfer is permitted but the Hall–Petch type relation still holds true. Hence the grain boundaries are assumed to be impenetrable to dislocations. The smallest grain size is still larger than the inverse Hall-Petch regime [19,32], hence grain boundary sliding is not considered here.

2.2 Calculation of dislocation configurational energy density

The calculation of dislocation configurational energy has been described in the earlier paper [8], hence is only covered briefly here.

During the plastic deformation, the free energy Φ stored in the material consists of the elastic stored energy W^e and the energy stored in the dislocations W^{dis}, i.e.

$$\Phi = W^e + W^{dis} \tag{4}$$

The free energy of a specimen with volume V in DDP is given by

$$\Phi = \frac{1}{2}\int_V (\tilde{\boldsymbol{\sigma}} + \hat{\boldsymbol{\sigma}}) : (\tilde{\boldsymbol{\varepsilon}} + \hat{\boldsymbol{\varepsilon}}) dV \tag{5}$$

Lubarda et al. [33] introduced an exclusion procedure to calculate the stress and strain field in a model which contains singularities from dislocations. The resultant free energy is thus given by

$$\Phi = \frac{1}{2}\int_V \hat{\boldsymbol{\sigma}} : \hat{\boldsymbol{\varepsilon}} dV + \frac{1}{2}\int_V (\hat{\boldsymbol{\sigma}} : \tilde{\boldsymbol{\varepsilon}} + \tilde{\boldsymbol{\sigma}} : \hat{\boldsymbol{\varepsilon}}) dV + \frac{1}{2}\sum_{\substack{j=1 \\ j\neq k}}^{N}\sum_{k=1}^{N}\int_V \tilde{\boldsymbol{\sigma}}^j : \tilde{\boldsymbol{\varepsilon}}^k dV + E_l \tag{6}$$

where E_l is the sum of all dislocation line energies as they are isolated in an infinite matrix, which includes the self and core energy. The calculation of E_l is derived in [7].

The elastic stored energy at each stage of loading is written as

$$W^e = \frac{1}{2}\int_V \breve{\boldsymbol{\sigma}} : \breve{\boldsymbol{\varepsilon}} dV \tag{7}$$

in which $\breve{\boldsymbol{\sigma}}$ and $\breve{\boldsymbol{\varepsilon}}$ are the stress and strain fields respectively in a dislocation-free body with the traction $\boldsymbol{T} = \hat{\boldsymbol{T}} + \tilde{\boldsymbol{T}}$ applied on the external surfaces of the model [5,6].

The energy stored in the dislocations W^{dis} consists of the dislocation line energy E_l and dislocation configurational energy E_{conf} which is the extra energy stored in the dislocation structure. The configurational energy can be determined readily by substituting Eq. (6)~(7) to Eq.(4) as

$$E_{conf} = \frac{1}{2}\int_V \widehat{\boldsymbol{\sigma}}:\widehat{\boldsymbol{\varepsilon}}dV + \frac{1}{2}\int_V (\widehat{\boldsymbol{\sigma}}:\tilde{\boldsymbol{\varepsilon}} + \tilde{\boldsymbol{\sigma}}:\widehat{\boldsymbol{\varepsilon}})dV + \frac{1}{2}\sum_{\substack{j=1 \\ j\neq k}}^{N}\sum_{k=1}^{N}\int_V \tilde{\boldsymbol{\sigma}}^{\boldsymbol{j}}:\tilde{\boldsymbol{\varepsilon}}^{\boldsymbol{k}}dV - \frac{1}{2}\int_V \breve{\boldsymbol{\sigma}}:\breve{\boldsymbol{\varepsilon}}dV \quad (8)$$

The spatial distribution of configurational energy volumetric density U_{conf} can be determined analogously as

$$U_{conf} = \frac{1}{2}\widehat{\boldsymbol{\sigma}}:\widehat{\boldsymbol{\varepsilon}} + \frac{1}{2}(\widehat{\boldsymbol{\sigma}}:\tilde{\boldsymbol{\varepsilon}} + \tilde{\boldsymbol{\sigma}}:\widehat{\boldsymbol{\varepsilon}}) + \frac{1}{2}\sum_{\substack{j=1 \\ j\neq k}}^{N}\sum_{k=1}^{N}\tilde{\boldsymbol{\sigma}}^{j}:\tilde{\boldsymbol{\varepsilon}}^{k} - \frac{1}{2}\breve{\boldsymbol{\sigma}}:\breve{\boldsymbol{\varepsilon}} \quad (9)$$

Additionally, the configurational energy area density G_{conf} is defined as

$$G_{conf} = \frac{U_{conf}}{\sqrt{\rho_{dis}}} \quad (10)$$

where ρ_{dis} is the local dislocation density. Note that the dislocation configurational energy can also be described in the entropy function in the general free energy expression as by Berdichevsky [38,39]. In this work, we focus on the effect of the microstructure (modelling) parameters on the evolution and distribution of the configurational energy area density.

3. Numerical results

The overall stress versus strain responses of model specimens with different properties are first assessed as shown in Fig. 2. For polycrystals with LSD and single crystal orientation in all grains (equivalent to a single crystal with several impenetrable boundaries), a classic size effect is observed from the four curves in Fig. 2(a): the flow stress is higher in small grain size; similar observations which follow the Hall-Petch relationship have been reported by Nicola et al. [40]. This phenomenon is only significant when the grain size is smaller than $2.0\mu m^2$, beyond which the difference between the overall stress response is negligible. In all calculations, there is an initial stress drop after the emission of the first dipole which results from the burst of dislocation emission [14]. Deshpande et al. [5] demonstrated that using higher value of the standard deviation for source strength, the transition from the elastic to the plastic response is smoothed but the response in the fully plastic regime is not significantly affected. The stress drop is smaller and the hardening is stronger in the specimen of smaller grain size because the movement of dislocations is hindered by high grain boundary densities. In other words, the mean free distance of dislocations is shorter for small grain size and the material is more difficult to deform plastically.

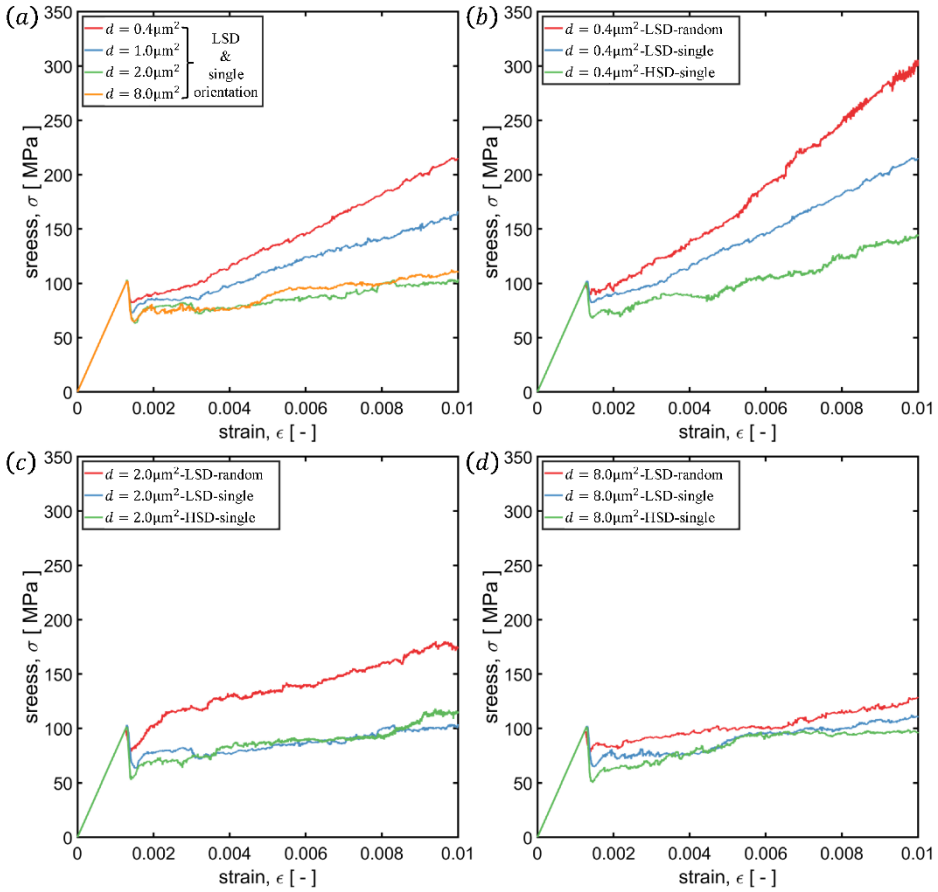

Fig. 2. Tensile response of polycrystals with hexagonal grains. (a) LSD and single orientation (i.e. single crystal with boundaries) in all grains and the grain size varies from $0.4\mu m^2$ to $8.0\mu m^2$; comparison of stress-strain responses for different source density and crystal orientation (b) $d = 0.4\mu m^2$; (c) $d = 2.0\mu m^2$ and (d) $d = 8.0\mu m^2$.

In addition to the grain size, the source density and crystal orientation also play a significant role in determining the overall stress response. For the $d = 0.4\mu m^2$ specimens in Fig. 2(b), both source density and crystal orientations affect the hardening rate significantly. Low source density leads to a strong hardening because the generated dislocations are not sufficient to accommodate the remote loading, hence the stress is built up faster with further loading. This observation is consistent with the 3D DDP simulations of Cu micro-pillar compression [41] which demonstrated that the hardening rate is larger in smaller pillars with lower dislocation storages. In contrast, the specimen with high source density generally shows a low flow stress and weak hardening as more dislocations are emitted. For the same reason, the initial stress drop for HSD is large because there are more sources activated simultaneously which leads to the sudden burst of dislocation emission.

With increasing the grain size, the influence of source density and crystal orientations reduce. As shown in Fig. 2(c-d), there is little difference between the LSD and HSD specimens when the grain size is beyond the size-dependent regime (e.g. $d \geq 2.0\mu m^2$). The mean free distance of dislocations in these specimens is large enough for slip to occur and accommodate the deformation. For the $d = 2.0\mu m^2$ specimens, the one with random orientation still displays a higher flow stress than the others. This effect levels off in the larger specimen as there are more low strength sources in the low Schmid factor grains and slip is able to initiate in these grains at lower stress.

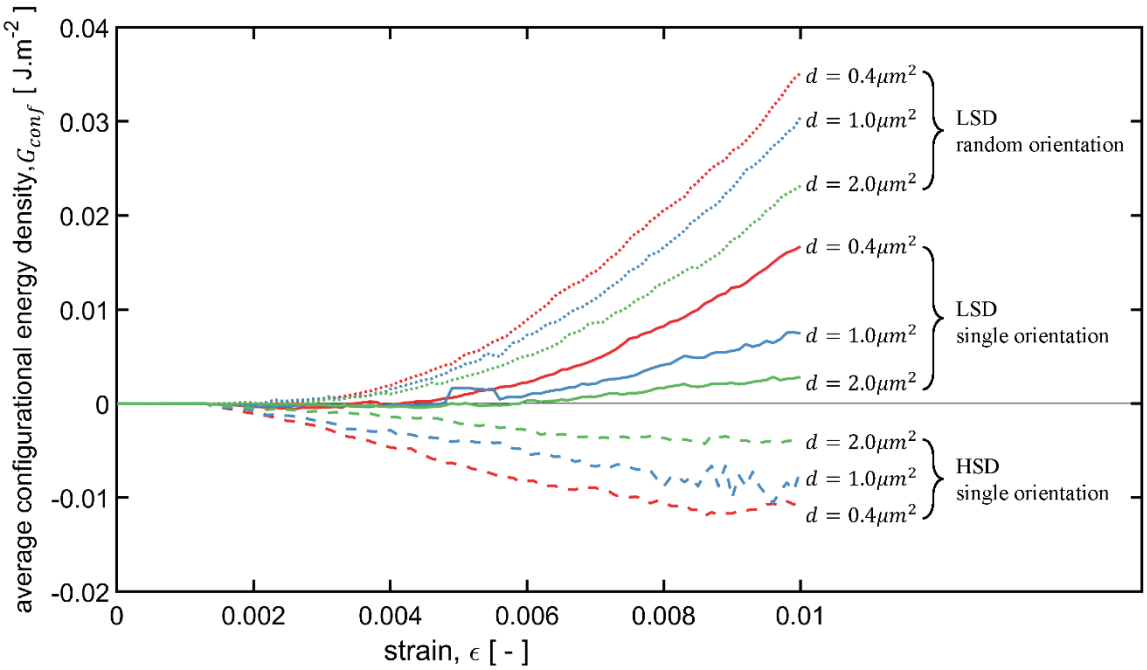

Fig. 3. Average configurational area density evolution with strain. Curves are shown for selected values of the modelling parameters

The evolutions of the average configurational area density of specimens with different modelling parameters are plotted in Fig. 3. The first observation is that a similar size dependence response is observed in G_{conf}: the absolute magnitude of configurational energy density is larger in small grain sized specimens. In addition, the LSD specimens display positive configurational energy densities while the HSD specimens show negative values, which means that there is extra energy stored in the LSD specimens to maintain the dislocation structure and the dislocation structure for HSD specimens is more stable than that of isolated dislocations. For the specimens with the single crystal orientation and the same grain size, the average configurational energy of LSD and HSD at 1% strain is similar in magnitude but opposite in sign. However, at the onset of plasticity, the configurational energy density establishes faster in HSD because more dislocations are emitted corresponding to a bigger stress drop in Fig. 2(b-d).

In order to understand the differences in the configurational energy density between specimens, the spatial distributions of configurational energy density at 1% strain of are shown in Fig. 4 together with the corresponding dislocation structure. Comparing Fig. 4(b) and (d), there are obviously more dislocations in the HSD specimen and most of them are piling up near the grain boundaries. The energy density distribution in Fig. 4(a) is highly localised at the boundaries and this corresponding to the dislocation pile ups in Fig. 4(b). The average energy density level are lower in the HSD specimen because the deformation is accommodated by the generation and the movement of large amount dislocations and the overall stress level is lower. Since the grain boundaries are impenetrable, little energy is dissipated as heat et al. and the external work done is mainly transferred as elastic stored energy and dislocation-associated energy, the latter is mainly presented in the material as dislocation line energy. It worth noting that there are several positive high energy spots located near the triple junctions in Fig. 4(c) even though the overall energy density is negative.

For the specimens with large grain size, there are quite amount of dislocations remain inside the grains for both LSD and HSD specimens. They are either piling up against obstacles or trapped at the intersection point of two slip planes. As a result, high energy spots are observed within grains and at

grain boundaries. The overall distributions for LSD and HSD in large grains are similar to small grains but the differences are less distinct.

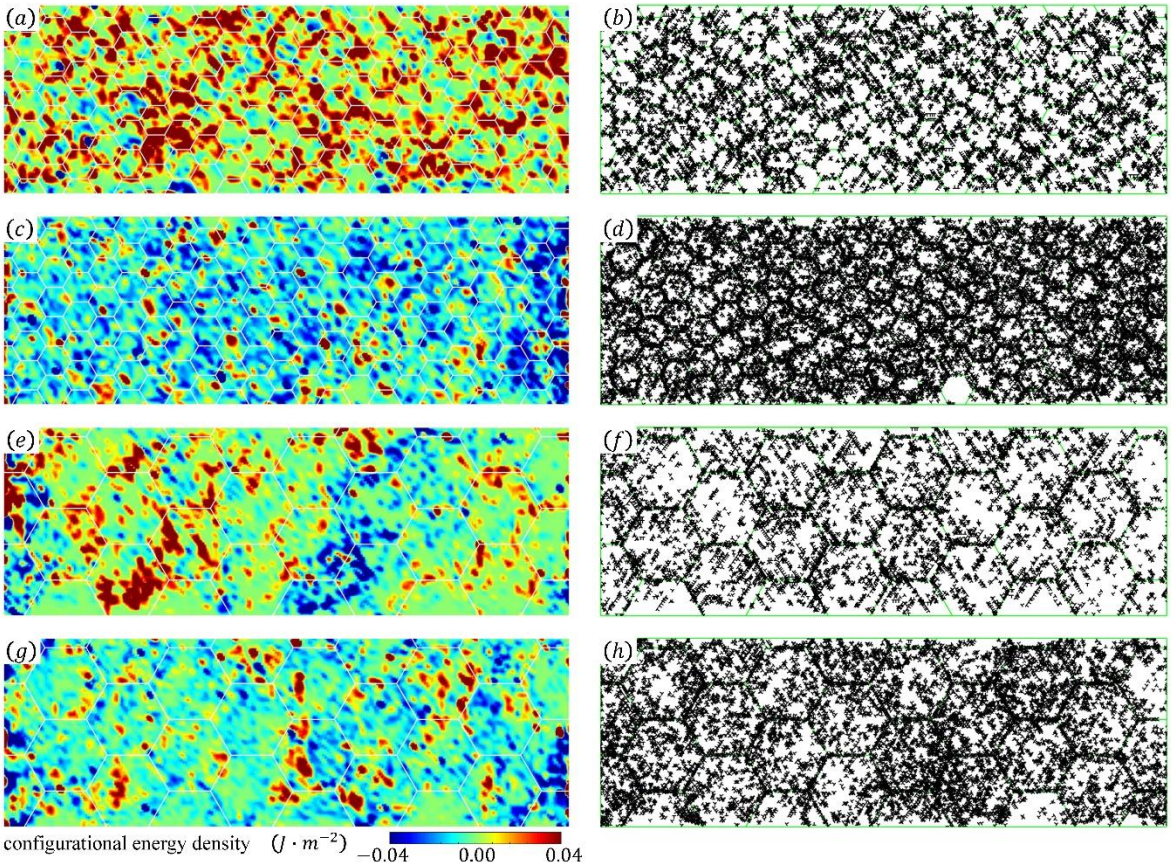

Fig. 4. The distribution of dislocation configurational area density and the corresponding dislocation structure at 1% strain. (a/b) $d = 0.4\mu m^2$ with LSD; (c/d) $d = 0.4\mu m^2$ with HSD; (e/f) $d = 8.0\mu m^2$ with LSD; (g/h) $d = 8.0\mu m^2$ with HSD.

The configurational energy stored in the dislocation structure highly depends on the distance between dislocations. In order to investigate this dependence, we calculate the average dislocation distance r_{dis} during loading as a function of the overall dislocation density $\bar{\rho}_{dis}$ given by

$$r_{dis} = \frac{1}{\sqrt{\bar{\rho}_{dis}}} \tag{11}$$

The evolution of configurational energy area density against the dislocation spacing is shown in Fig. 5. With increasing deformation, the average dislocation spacing reduces in all specimens because the rate of emission is higher than that of annihilations which results in more dislocations in the system. For the specimens with the same grain size, the LSD cases display longer dislocation distances and higher energy densities especially for the random orientation. To explain this phenomenon, the evolution of dislocation structure is shown schematically in Fig. 6 for LSD and HSD cases. Assume a group of dislocations are emitted from a weak source (whose strength is lower than the average value) in one grain and pile up at the grain boundary, resulting from which, stress concentration occurs as the grey region in Fig. 6. For the LSD case, there is lower chance that sources located in the neighbouring grain exist in that region, hence they may not be activated from the stress concentration (but might be activated later due to the hardening effect). A positive configurational energy density region forms as a result and continues to increase with further loading. The average dislocation spacing in this case is

larger. On the other hand, for the HSD specimen, the chance for sources located in the high stress region to exist is higher. These sources are activated before the overall stress exceeds the source strength. Opposite-signed pile ups are formed against the same boundary in the neighbouring grain and the local stress is reduced. The energy stored in the primary pile up is thus released. Since the overall dislocation density is higher in the HSD specimen, the average dislocation spacing is smaller. Interestingly the hardening rate for the HSD case is lower compare to LSD (Fig. 2). The high dislocation density in the HSD specimen under a high strain rate accommodates the remote loading better, which leads to a lower hardening rate.

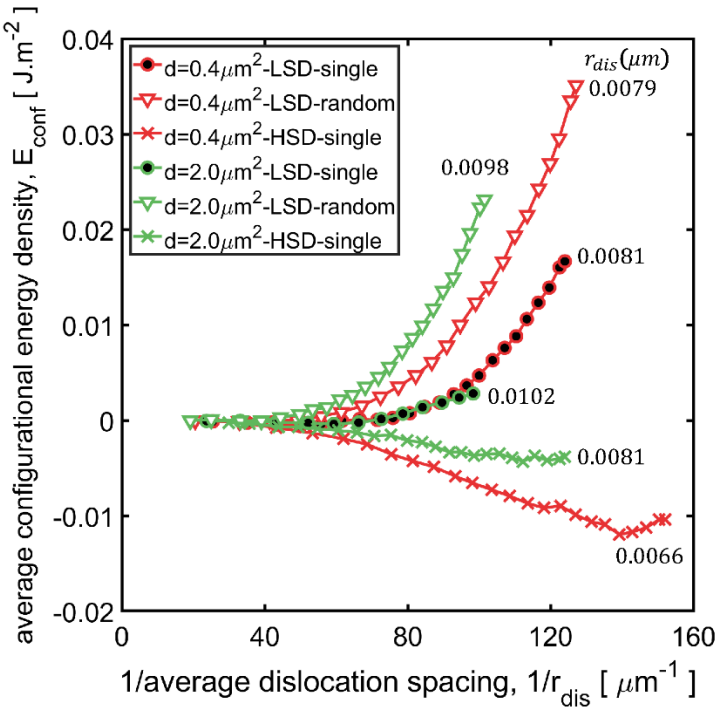

Fig. 5. Dependence of the average configurational energy G_{conf} on the average dislocation spacing r_{dis}.

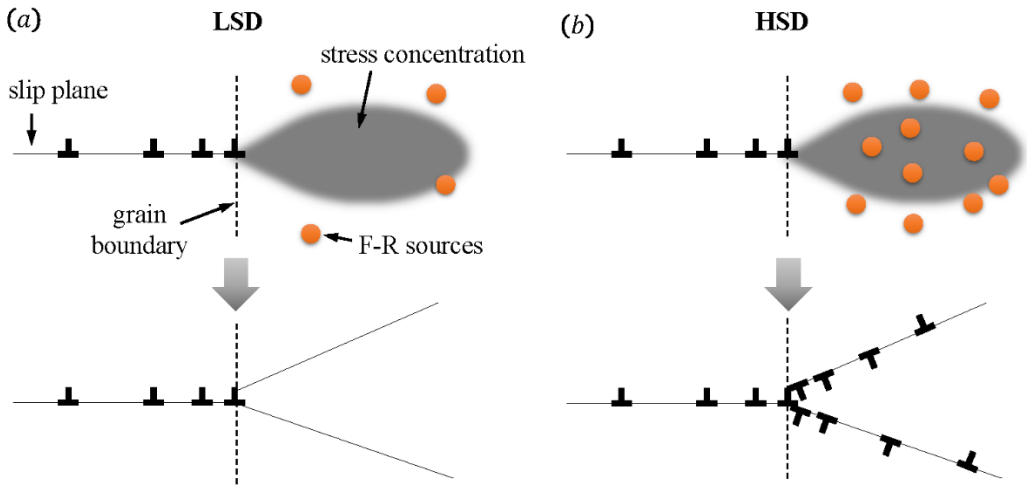

Fig. 6. Schematic illustration of dislocation structure evolution in (a) LSD specimen and (b) HSD specimen.

The activation of a Frank-Read source due to the stress concentration from a pile-up in the neighbouring grain (named as indirect slip transfer [30], in contrast to direct dislocation transmission through the boundary) in the $d = 8.0\mu m^2$ with HSD specimen is shown in Fig. 7. When the applied strain is 0.257%, a pile-up of dislocations builds up against the grain boundary and a region of high stress is developed. When the applied strain reaches 0.259%, the average spacing between the dislocations in the pile-up becomes shorter and the stress in front of it is higher. As a result, the Frank-Read source located near the high-stress region is activated. With further loading, the stress concentration may reduce due to the newly generated dislocations.

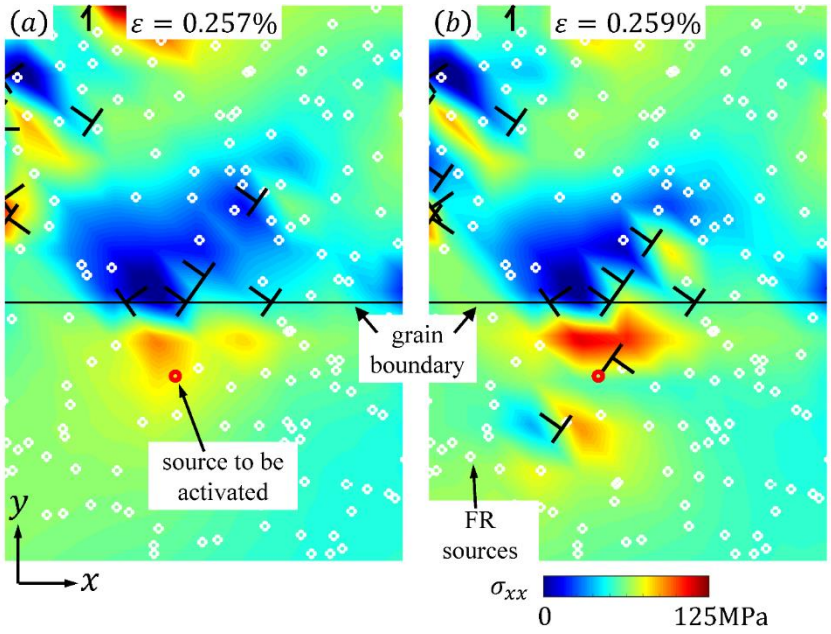

Fig. 7. Stress distribution of $d = 8.0\mu m^2$ with HSD specimen showing the activation of a Frank-Read source due to the stress concentration from a pile-up in the neighbouring grain. (a) Before the indirect slip transfer at $\varepsilon = 0.257\%$ and (b) after the indirect slip transfer at $\varepsilon = 0.259\%$.

The evolution of configurational energy density in Fig. 3 and Fig. 5 demonstrates that a random orientation results in about twice the energy of that in the specimen with single orientation, although the resultant dislocation spacing is similar. To further investigate the effect of crystal orientation, we consider three additional $d = 0.4\mu m^2$ specimens with controlled misorientations. The misorientation angles $\Delta\theta$ between the neighbouring grains are assigned with a checker-board arrangement, i.e. every neighbouring two grains are assigned with the orientations as $\varphi^{(1)} = 0^o$ and $\varphi^{(1)} = \Delta\theta$. The configurational energy area density at 1% strain against the misorientation angle are summarised in Fig. 8. Interestingly the misorientation angle does not significantly affect the average dislocation spacing, i.e. the value is about $0.008\mu m$ in all cases. However, the configurational energy density is higher with increasing misorientation. A 10^o misorientation angle specimen displays about $0.03J \cdot m^{-2}$ energy density, which is much higher than $0.017J \cdot m^{-2}$ for the single orientation (single crystal with boundaries). There is a slightly increased energy density when the angle increases to 30^o and the random orientation specimen shows the highest energy density. The overall stress response shows a similar trend as the configurational energy density. The configurational energy stored in the dislocation structure does not only depend on the relative position of the dislocations in the pile up, but is also related to the local stress status. For the same dislocation structure, it may be more difficult to maintain that configuration under one stress status but may be energetically preferred under another, and the

configurational energy density in the latter is thus lower. For the $d = 0.4\mu m^2$ specimens investigated in Fig. 8, the configurational energy area density under higher stress is higher which implies more energy is stored in the dislocation structure during deformation.

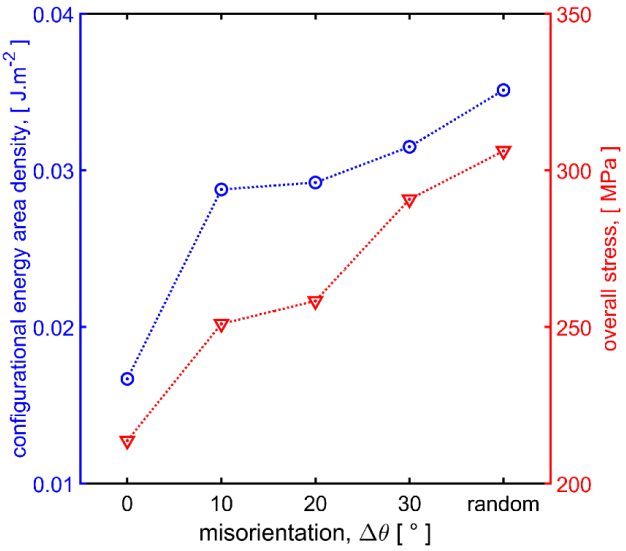

Fig. 8. The variation of the average configurational area density and the overall stress at 1% strain with misorientation angle $\Delta\theta$ in the $d = 0.4\mu m^2$ specimens.

4. Conclusions

We have carried out systematic analysis of dislocation configurational energy density in BCC polycrystals under uniaxial tension conditions. The effect of grain size, source density and misorientation on the configurational energy density evolution are investigated using hexagonal grains.

(1) Classic size-dependent stress responses are observed between $d = 0.4\mu m^2$ to $8.0\mu m^2$. The effects of source density and crystal orientation are stronger in smaller grains and the effects are negligible for the grain size of $8.0\mu m^2$.

(2) The average configurational energy area density displays a size-dependent response: the absolute magnitude is higher in small grains. LSD specimens show positive overall configurational energy density while HSD leads to negative values. The average dislocation spacing in the latter is shorter. Higher (positive) configurational energies are associated with earlier fatigue crack nucleation in crystal plasticity studies [9–13].

(3) Configurational energy area density is also a function of the local stresses. Differences in crystal misorientations result in different stress responses. The configurational energy area density is higher in the specimens with random orientation (high stress) and lower in those with single orientation.

Acknowledgements

Financial support from the Engineering and Physical Sciences Research Council through the HexMat programme grant EP/K034332/1 is gratefully acknowledged. ZZ would like to acknowledge the support from NSFC (Grants 91860130). FPED wishes to acknowledge gratefully the provision of funding for his Royal Academy of Engineering/Rolls-Royce research chair.

References

1. N. M. Ghoniem, S.-H. Tong, and L. Z. Sun, Phys. Rev. B **61**, 913 (2000).

2. L. . Sun, N. . Ghoniem, S.-H. Tong, and B. . Singh, J. Nucl. Mater. **283**–**287**, 741 (2000).

3. H. M. Zbib, T. Diaz de la Rubia, and V. Bulatov, J. Eng. Mater. Technol. **124**, 78 (2001).

4. H. M. Zbib and T. Diaz de la Rubia, Int. J. Plast. **18**, 1133 (2002).

5. V. S. Deshpande, A. Needleman, and E. Van der Giessen, J. Mech. Phys. Solids **53**, 2661 (2005).

6. D. S. Balint, V. S. Deshpande, A. Needleman, and E. Van der Giessen, Int. J. Plast. **24**, 2149 (2008).

7. A. A. Benzerga, Y. Bréchet, A. Needleman, and E. Van der Giessen, Acta Mater. **53**, 4765 (2005).

8. Z. Zheng, N. G. Prastiti, D. S. Balint, and F. P. E. Dunne, J. Mech. Phys. Solids **In Press**, (2019).

9. V. V. C. Wan, J. Jiang, D. W. MacLachlan, and F. P. E. Dunne, Int. J. Fatigue **90**, 181 (2016).

10. B. Chen, J. Jiang, and F. P. E. Dunne, Int. J. Plast. **101**, 213 (2018).

11. B. Chen, J. Jiang, and F. P. E. Dunne, J. Mech. Phys. Solids **106**, 15 (2017).

12. D. Wilson, Z. Zheng, and F. P. E. Dunne, J. Mech. Phys. Solids **121**, 147 (2018).

13. D. Wilson, W. Wan, and F. P. E. Dunne, J. Mech. Phys. Solids **126**, 204 (2019).

14. D. S. Balint, V. S. Deshpande, A. Needleman, and E. Van der Giessen, Model. Simul. Mater. Sci. Eng. **14**, 409 (2006).

15. B. Kondori, A. Needleman, and A. Amine Benzerga, J. Mech. Phys. Solids **101**, 223 (2017).

16. E. Tarleton, D. S. Balint, J. Gong, and A. J. Wilkinson, Acta Mater. **88**, 271 (2015).

17. D. S. Balint, V. S. Deshpande, A. Needleman, and E. Van der Giessen, J. Mech. Phys. Solids **54**, 2281 (2006).

18. H. H. M. Cleveringa, E. Van der Giessen, and A. Needleman, Int. J. Plast. **15**, 837 (1999).

19. S. S. Quek, Z. H. Chooi, Z. Wu, Y. W. Zhang, and D. J. Srolovitz, J. Mech. Phys. Solids **88**, 252 (2016).

20. V. V. C. Wan, D. W. MacLachlan, and F. P. E. Dunne, Int. J. Fatigue **68**, 90 (2014).

21. S. B. Biner and J. R. Morris, Philos. Mag. **83**, 3677 (2003).

22. H. Abdolvand, J. Wright, and A. J. Wilkinson, Nat. Commun. **9**, 171 (2018).

23. C. Zhang, H. Li, P. Eisenlohr, W. Liu, C. J. Boehlert, M. A. Crimp, and T. R. Bieler, Int. J. Plast. **69**, 21 (2015).

24. E. Van der Giessen and A. Needleman, Model. Simul. Mater. Sci. Eng. **3**, 689 (1995).

25. H. H. M. Cleveringa, E. Van der Giessen, and A. Needleman, J. Mech. Phys. Solids **48**, 1133 (2000).

26. W. A. Curtin, V. S. Deshpande, A. Needleman, E. Van der Giessen, and M. Wallin, Int. J. Fatigue **32**, 1511 (2010).

27. J. R. Rice, Mech. Mater. **6**, 317 (1987).

28. A. A. Benzerga, Y. Bréchet, A. Needleman, and E. Van der Giessen, Model. Simul. Mater. Sci. Eng. **12**, 159 (2003).

29. S. S. Chakravarthy and W. A. Curtin, J. Mech. Phys. Solids **58**, 625 (2010).

30. Z. Zheng, D. S. Balint, and F. P. E. Dunne, Acta Mater. **127**, 43 (2017).

31. Z. Li, C. Hou, M. Huang, and C. Ouyang, Comput. Mater. Sci. **46**, 1124 (2009).

32. S. S. Quek, Z. Wu, Y. W. Zhang, and D. J. Srolovitz, Acta Mater. **75**, 92 (2014).

33. V. A. Lubarda, J. A. Blume, and A. Needleman, Acta Metall. Mater. **41**, 625 (1993).